66-14,235

MULLIS, Jr., Charles Howell, 1926-
TURBULENT FLOW TRACTIVE FORCES ON GRANULAR BED MATERIALS.

The University of Oklahoma, Ph.D., 1966
Engineering, civil

THE UNIVERSITY OF OKLAHOMA

GRADUATE COLLEGE

TURBULENT FLOW TRACTIVE FORCES ON GRANULAR BED MATERIALS

A DISSERTATION

SUBMITTED TO THE GRADUATE FACULTY

in partial fulfillment of the requirements for the

degree of

DOCTOR OF PHILOSOPHY

BY

CHARLES HOWELL MULLIS, JR.

Norman, Oklahoma

1966

TURBULENT FLOW TRACTIVE FORCES ON GRANULAR BED MATERIALS

APPROVED BY

DISSERTATION COMMITTEE

ACKNOWLEDGEMENT

The writer would like to express his sincere appreciation to his dissertation director, Dr. J. F. Harp for the cooperation, encouragement and assistance during the course of this work.

This project was financed in part by the National Science Foundation under NSF Grant GK-322. In addition, the writer was able to undertake this program because of the financial assistance afforded by a Ford Foundation loan. To both these agencies, the writer is deeply grateful.

Messrs. Gustavo H. Garcia and G. N. S. Rao acted as technical assistants during portions of this project. The writer would like to acknowledge their valuable assistance and express his thanks.

Finally, the writer would like to express his very deep thanks to his wife, Kay, for her general encouragement during this period of his life and specifically for her typing of this manuscript.

ABSTRACT

Utilizing velocity distribution formulae developed by Christensen, a theoretical method for computing critical tractive shear stresses on a uniform, cohesionless bed-material under rough regime flow conditions is presented.

A laboratory flat bed flume was constructed and measurements were made of the critical tractive shear stresses on both a washed bank-run, quartz sand and on gypsum sand. These two types of sand allowed a study to be made of the effects of differing specific gravities on the problem. The shear stresses were measured by the Preston technique and evaluated by means of calibration curves developed by Laursen and Hwang.

The theoretical and experimental results were compared and found to correlate qualitatively.

The experimental results were also compared with the results obtained by Shields, White and Harp. All experimental results correlated favorably in a qualitative manner except for Shields. No justification was found to use the classical Shields' diagram as a basis for comparison.

TABLE OF CONTENTS

LIST OF ILLUSTRATIONS

LIST OF TABLES

LIST OF SYMBOLS

Symbol	Nomenclature
A	Cross-sectional area of particle, ft^2.
C_d	Drag coefficient.
c_i	Mathematical constant.
d	Particle diameter, ft; or differential operator.
F_A	Aerodynamic lift force, lb.
F_B	Buoyant force, lb.
F_D	Drag force, lb.
$F_{x,y}$	Force components, lb.
g	Acceleration due to gravity, ft/sec/sec.
h	Distance from datum to center of exposed particle, ft.
K	$= \frac{K_s v_*}{\nu}$.
k_s	Particle roughness, ft.
ℓ_i	Moment arms for the respective forces, ft.
ln	Natural logarithm.
N	Normal force, lb.
Q	Flow rate, cu. ft/sec.
v	Point velocity, ft/sec.
V_{ave}	Average velocity, ft/sec.
V_{cr}	Critical velocity, ft/sec.

$V_{m,cr}$	Mean critical velocity, ft/sec.
v_*	$=\sqrt{\tau_o/\rho}$, the shear velocity, ft/sec.
~~V~~	Volume, cu ft.
W	Particle weight, lb.
x	A random variable.
y	Distance from datum to point where velocity is being evaluated.
Y	$= \frac{y v_*}{\nu}$.
α	Shape factor for volume.
α_s	Shape factor for area.
β_i	Mathematical coefficients.
Γ	The gamma function (mathematics).
γ	Unit weight of water, lb/cu ft.
γ_s	Unit weight of bed material, lb/cu ft.
Δ	A finite difference (mathematics).
δ'	Thickness of laminar boundary layer, ft.
ν	Kinematic viscosity, ft^2/sec.
ρ	Mass density, slugs/cu ft.
τ_s	Shearing stress, lb/sq ft.
τ_o	Critical shearing stress, lb/sq ft.
θ	Angle between the line of action of the normal force and the vertical.

TURBULENT FLOW TRACTIVE FORCES ON GRANULAR BED MATERIALS

CHAPTER I

INTRODUCTION

Statement of the Problem

Sediment, and the forces acting on sediment, are two of the most important problems an engineer must solve when he designs any works involving clear or turbid waters on the earth's surface.

The forces acting on sediment can be thought of as two distinct types: One is an erosive force that acts on sediment by lifting or moving it in a generally downstream direction. This action is commonly called scour. The other class can be thought of as a negative force causing negative scour or deposition. When deposition occurs, sediment is withdrawn from suspension or its downstream movement ceases and the sediment comes to rest on the channel bottom.

Various phases of the sediment problem occur when an engineer designs such works as drainage or irrigation channels, the improvement of existing waterways or engages in the planning of reservoirs and the improvement of harbors. The problem is constantly being confronted in the control of soil erosion on conservation watersheds.

When the general downstream movement of sediment occurs, engineers speak of this movement in terms of transport loads. Transport loads occur in any combination of the basic types of loadings. These are primarily:

The bed load and the suspended load. The bed load consists of the coarse material moving on or near the bed. It is subdivided into the contact load, which is that material rolled or slid along the bed in substantially continuous contact with the bed; and the saltation load, which is the material bouncing along the bed, or moved, directly or indirectly , by impact of the bouncing particles. The suspended load is the material moving in suspension in a fluid, being kept up by the upward components of the turbulent currents or by colloidal suspension. A load term which is frequently used is the wash load. The wash load is defined as that part of the sediment load of a stream which is composed of particle sizes smaller than those found in appreciable quantities in the shifting portions of the stream bed.

In this study, interest is centered on the problem at the instant in time just before any of the grains physically move in what ever type loading will ultimately occur. Experimentally, the tractive shear stress causing incipient movement will be measured by the Preston shear technique. A theoretical analysis of the same problem will be made and the results compared. A unique feature of both the experimental and theoretical analysis is that no use is made of the slope of the energy grade line in the problem. Instead, the Newtonian drag force concept is utilized, and forces acting at a point are evaluated.

Historical Background

For centuries engineers have recognized this problem and have expended considerable time and thought to its solution. A brief historical evolution of the analytical and experimental work that has been done in this field will be given here. The reader who would like to further ex-

plore this development is invited to read the work of S. Leliavsky (1.1)- parenthetical numbers refer to the bibliography.

Most investigators directed their efforts towards one of two approaches to the problem. These were the critical velocity approach or the critical shear approach.

The critical velocity may be defined as that velocity near the channel bed above which some bottom sediment will exhibit instability and movement.

In 1753, the first published analysis of this line of thinking was made by A. Brahms. He coined the term "critical velocity" and expressed it mathematically as

$$V_{cr} = \text{const.}\ W^{1/6}$$

where V_{cr} is the critical velocity and W is the submerged weight of the particle.

In 1834, this same formula was derived independently by W. Airy. These derivations are now commonly called the Brahms-Airy Law.

In 1930, a similar law was proposed by G. Lacy (1.2).

Many empirical tables have been developed by engineers, e.g., L. G. DuBuat (1.3), which give the magnitude of bed pick-up velocity as a function of the size and shape of the grains being acted upon.

Another critical velocity approach was made by analyzing the critical velocity in terms of the mean velocity of the channel cross-section.

Probably the best known and most often misused results were those presented by R. G. Kennedy in 1895. Kennedy based his conclusions on studies made of large irrigation works in India. His relationship was that

$$V_{m,cr} = c_1 h_o^{c_2}$$

where $V_{m,cr}$ is the mean velocity of the cross-section when movement starts; h_o is the water depth and c_1 and c_2 are empirical constants which are functions of the bed material. Based on his observations in India, Kennedy proposed $c_2 = 0.64$ and $c_1 = 0.82$ for light sandy material and $c_1 = 1.07$ for coarse sandy material. Since that time, other observers have attempted to refine the values for c_1 and c_2.

As a result of Kennedy's and other investigators' work done mainly in India, the Regime Theory for silty and stable channels was developed. This theory is almost exclusively empirical in nature. Sir Claude Inglis compiled a complete resume of this work (1.4).

It was finally realized by many engineers that the critical velocity approach left much to be desired. Finally in the 1930's, investigators in the United States and in Europe started studying the problem using the critical shear stress approach. Most investigators felt that the critical shear stress was a function of the grain size. Many investigations were undertaken to study these relationships. L. G. Straub (1.5) summarized these results and published tables of these relationships. These tables are still widely used by designers today. E. W. Lane (1.6) also gave a survey of the empirical values of the critical shear stress.

Several mildly conflicting definitions of the critical shear stress have been presented by different investigators. A simplified definition of the critical shear stress would be the temporal spatial average intensity of shear when the more exposed particles are moved by the fluid forces at a maximum.

In 1936, A. Shields (1.7) published the results of his work. He assumed that the problem had no analytical solution. Therefore he made

certain gross assumptions and then substantiated them or modified them in accordance with his experimental results. These assumptions were based on the Prandtl-Karman velocity distribution law and the Newtonian drag concept. Shields presented no formal analytical expression describing his work. His relationships can only be expressed as functional notations with the form

$$\frac{\tau_o}{d\Delta\gamma} = \phi\left(\frac{d}{\delta'}\right).$$

The result of this work is the famous "Shields' diagram" against which all future work was compared as the standard. Shields' diagram is presented in Chapter IV of this report.

C. M. White, in 1940, (1.8) sought to determine the factors which govern incipient motion by equating the moments which tend to move the grains to those which resist the motion. White expressed his results in the form

$$\tau_o = K d \Delta\gamma .$$

White's results are presented graphically in Chapter IV.

The terms appearing in both Shields' and White's equations are explained in detail in Chapter IV - Analysis of Results.

In 1961, Christensen (1.9) made an exhaustive analytical study of most of the pertinent relationships involved in both soil and fluid mechanics. He isolated many important relationships and demonstrated that certain well-established relationships were not valid. He proposed counter-relationships to replace them. Several of these findings will be referred to later in the chapter dealing with theory.

A major breakthrough in the problem occurred in 1954. Preston (1.10) utilized the simple technique of measuring local surface-resistance

by means of a pitot tube resting on the boundary of a smooth surface. He utilized the pressure drop in a tube (the Preston tube) to calibrate his instrument. Preston obtained equations relating the intensity of shear to the pitot tube reading for the cases of the laminar sublayer enveloping the tube and for the tube in the turbulent boundary layer on the smooth surface.

In 1955, Hsu (1.11) extended the Preston shear method to cases where an adverse pressure gradient existed.

In 1962, Laursen and Hwang (1.12) extended the method to include rough boundaries.

These two studies (Hsu and Laursen and Hwang) completed the breakthrough started by Preston. They established the groundwork which would allow future investigators to explore the many facets of the total problem.

As an example, in 1963, Harp (1.13) related the average boundary shear to the incipient movement of sand particles on channel bottoms for both laminar and turbulent flow by use of the Preston shear technique.

Proposed Work of This Project

Borrowing the laboratory techniques developed by Harp and others, in the present study, the following objectives will be established:

1) Utilizing improvements in velocity distribution laws previously cited, an original theoretical analysis of the problem will be presented.
2) Tests will be conducted in which the Preston shear technique will be utilized to measure critical shear stresses with variables as follows:
    (a) Various gradations of cohesionless material will

be used.

(b) materials of different specific gravities will be used.

3) Theoretical and experimental results will be compared.

4) Experimental results will be compared with the Shields' "classic" diagram.

5) Conclusions will be drawn and recommendations will be presented for additional work that needs to be done on other aspects of this important problem.

CHAPTER II

THEORETICAL ANALYSIS OF THE PROBLEM

Component Parts of the Problem

Several investigators have attempted to develop a relationship between critical tractive shear stress and velocity parameters over a rather wide range of Reynolds numbers. In order to do this, they have all agreed that it was necessary to divide the problem into three distinct ranges.

1. A smooth range in which the soil particles were completely submerged within the laminar sub-layer, and, for all practical purposes, the boundary was smooth. ($d << \delta'$)
2. A transition range in which the particles protruded from or influenced the surface of the laminar sub-layer, thereby creating a semi-rough boundary. ($d \approx \delta'$)
3. A rough range in which the laminar sub-layer was extremely thin or disappeared altogether and a completely rough boundary was established. ($d >> \delta'$)

Velocity Distribution Laws

Traditionally, investigators used the Karman-Prandtl inner law to describe the velocity-shear stress relationship for the above three cases. The Karman-Prandtl inner law states that

$$\frac{v}{v_*} = 2.5 \ln \frac{y v_*}{\nu} + 5.5 = 2.5 \ln Y + 5.5$$

where the terms are described following Eqn. 2.2 below. Almost all investigators conceded that either of the two laws had serious shortcomings near the true boundary where the velocity had to be zero.

Christensen (op. cit.) analyzed these laws, determined why and how they failed and presented new laws to replace them. Christensen's new laws were valid over the entire range of use, worked at the true boundary and were simple enough that they could be used with ease.

It is felt that for almost every conceivable critical tractive shear stress problem with which the practicing civil engineer will be confronted, flow will exist in the rough flow range in open channel flow type problems. Thus it was decided to present a theoretical analysis of only that portion of the entire problem. For the interested reader who would like to pursue this line of analysis for the other two cases, it it recommended that the approach presented below be used. It is only necessary to substitute the appropriate velocity distribution criteria.

For the reader's additional information, Christensen's velocity distribution relationship is:

Smooth and transitional range

$$\frac{v}{v_*} = \beta_1 + 2.5 \ln [Y - (\beta_1 - 0.21)], \qquad \text{(Eqn. 2.1)}$$

and for the rough range,

$$\frac{v}{v_*} = 8.48 + 2.5 \ln \left(\frac{Y}{K} + 0.0338\right), \qquad \text{(Eqn. 2.2)}$$

Where v= point velocity at a distance y above the datum,

$$v_* = \sqrt{\tau_0/\rho},$$

$$Y = \frac{y v_*}{\nu},$$

$$K = \frac{K_s v_*}{\nu},$$

$$\beta_1 = \phi(K).$$

Therefore in the rough range (our area of interest),

$$\frac{v}{v_*} = 8.48 + 2.5 \ln\left(\frac{y}{K_s} + 0.0338\right).$$

Equations of Equilibrium when Motion Impends

To understand and analyze the concept of the critical tractive shear stress it is necessary to consider the free-body of a single exposed particle just as incipient motion impends. In Fig. 1 is shown such a free body with all forces acting on it.

We may now write the three equations of equilibrium for this body. These are:

$$\Sigma F_X = 0 = \tau_s A_s + F_D - N \sin\theta. \qquad \text{(Eqn. 2.3)}$$

$$\Sigma F_Y = 0 = F_A + F_B + N\cos\theta - W. \qquad \text{(Eqn. 2.4)}$$

$$\Sigma M_N = 0 = \tau_s A_s l_s - (W - F_B) l_w - F_A l_A + F_D l_D. \qquad \text{(Eqn. 2.5)}$$

Where

τ_s = shear stress

F_D = drag force

N = normal force

F_A = aerodynamic lift force

F_B = buoyant force

W = particle weight

A = area on which a stress acts

l = moment arms for the respective forces

θ = the angle the normal force makes with the vertical.

Eliminating the normal force and the aerodynamic lift force, we have

$$\tau_s + F_D \frac{(l_A \cot\theta + l_D)}{(A_s l_s + A_s l_A \cot\theta)} = (W - F_B)\frac{(l_w + l_A)}{(A_s l_s + A_s l_A \cot\theta)}. \qquad \text{(Eqn. 2.6)}$$

FIG. 1 FREEBODY OF TYPICAL SAND GRAIN

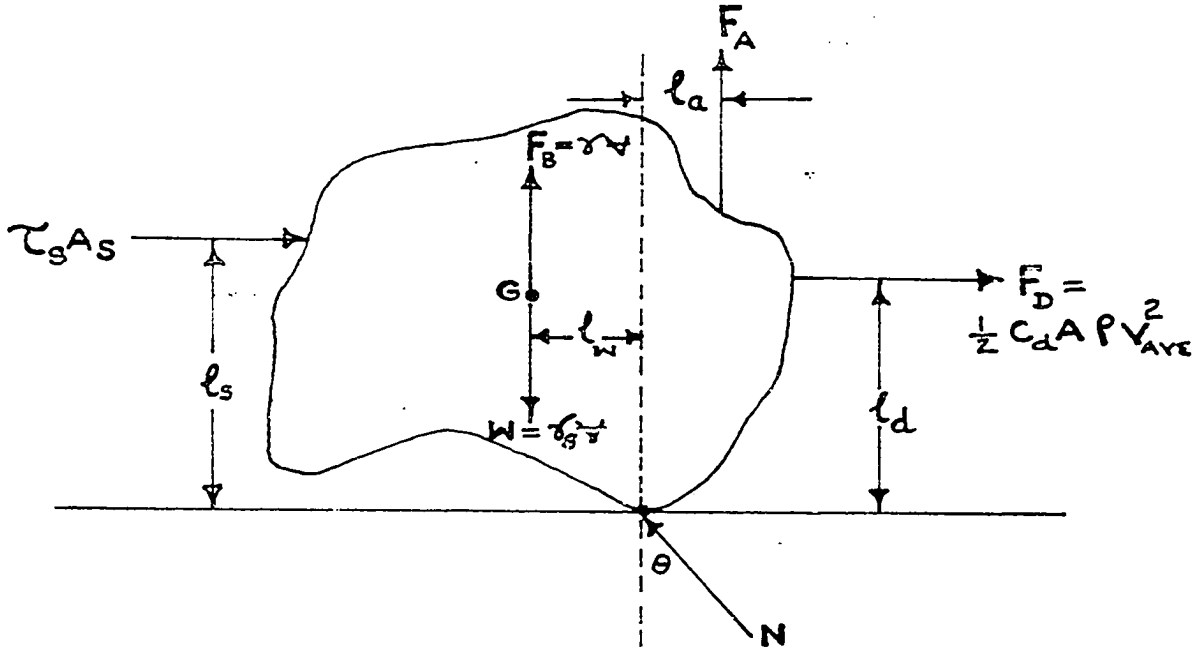

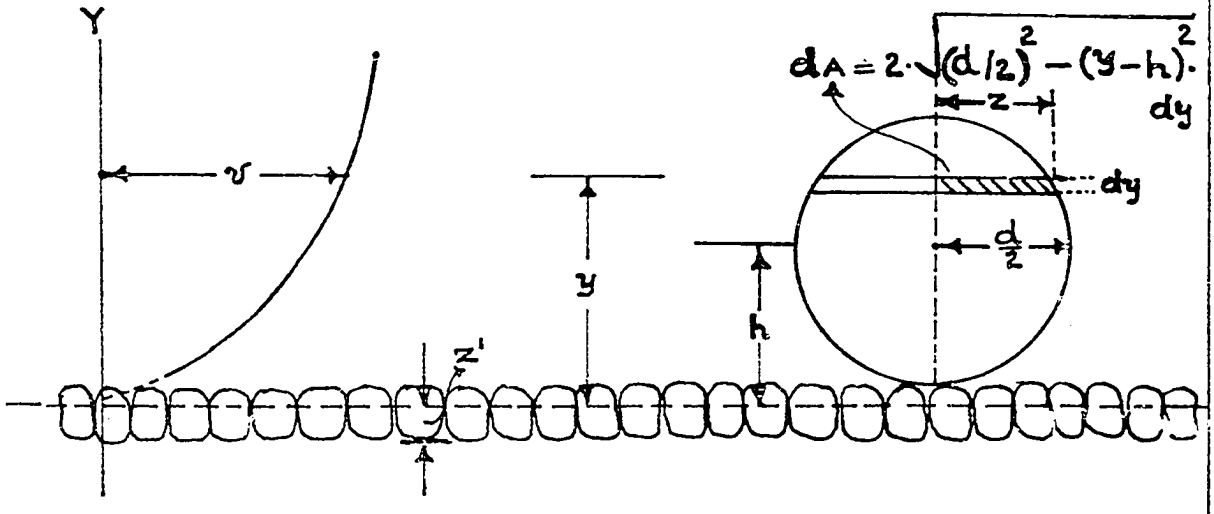

FIG. 2 TYPICAL PARTICLE (EXPOSED AND GREATLY EXAGGERATED IN SIZE)

Evaluating

$$W = \alpha d^3 \gamma_s \quad \text{and} \quad F_B = \alpha d^3 \gamma,$$

and

$$A_s = \alpha_s d^2,$$

where α and α_s are shape factors which will be discussed later and γ and γ_s are the unit weights of water and cohesionless bed materials respectively. We may rewrite Eqn. 2.6 in the following form:

$$\tau_s + \frac{F_D \beta_1}{\alpha_s d^2} = \frac{\alpha}{\alpha_s} d (\gamma_s - \gamma) \beta_2 . \qquad \text{(Eqn. 2.6A)}$$

where

$$\beta_1 = \frac{l_A \cot\theta + l_D}{l_s + l_A \cot\theta}$$

$$\beta_2 = \frac{(l_w + l_A)}{(l_s + l_A \cot\theta)}, \text{ and}$$

The classical evaluation of F_D has been

$$F_D = \frac{1}{2} C_D A \rho V_{AVE}^2, \qquad \text{(Eqn. 2.7)}$$

where C_D is the drag coefficient and

$$V_{AVE} = \frac{1}{A_T} \int_A v \, dA . \qquad \text{(Eqn. 2.8)}$$

Remembering that

$$\frac{v}{v_*} = 8.48 + 2.5 \ln \left(\frac{y}{k_s} + 0.0338 \right),$$

we may write

$$V_{AVE} = \frac{v_*}{A} \int_A \left[8.48 + 2.5 \ln \left(\frac{y}{k_s} + 0.0338 \right) \right] dA \qquad \text{(Eqn. 2.9)}$$

Referring to Fig. 2 we may rewrite Eqn. 2.9 after noting that

$$A_T = \alpha d^2$$

$$dA = 2 \sqrt{(d/2)^2 - (y - h)^2} \, dy,$$

$$y = h + d/2 \sin\theta,$$

$$dy = d/2 \cos\theta \, d\theta.$$

$$V_{AVE} = \frac{v_*}{\alpha d^2}\int_{h-d/2}^{h+d/2}\left[16.96 + 5\ln\left(\frac{y}{K_s} + 0.0338\right)\right]\sqrt{(d/2)^2 - (y-h)^2}\,dy$$

$$= \frac{v_*}{4\alpha}\int_{-\pi/2}^{\pi/2}\left[16.96 + 5\ln\left(\frac{h}{K_s} + 0.0338 + \frac{d}{2K_s}\sin\theta\right)\right]\cos^2\theta\,d\theta.$$

(Eqn. 2.10)

Then letting

$$A' = \frac{h}{K_s} + 0.0338 \quad \text{and} \quad B = \frac{d}{2K_s}, \text{ we have}$$

$$V_{AVE} = \frac{4.24\,v_*}{\alpha}\int_{-\pi/2}^{\pi/2}\cos^2\theta\,d\theta + \frac{5\,v_*}{4\alpha}\int_{-\pi/2}^{\pi/2}\ln(A + B\sin\theta)\cos^2\theta\,d\theta.$$

(Eqn. 2.11)

Now,

$$\frac{4.24\,v_*}{\alpha}\int_{-\pi/2}^{\pi/2}\cos^2\theta\,d\theta = \frac{2.12\,\pi\,v_*}{\alpha}.$$

It is now necessary to integrate, after changing integration limits,

$$\frac{5\,v_*}{8\alpha}\int_0^{2\pi}\left[\ln(A + B\sin\theta)\right]\cos^2\theta\,d\theta = f(\theta).$$

Let us rewrite in the form

$$K\int_0^{2\pi}\left[\ln A + \ln\left(1 + \frac{B}{A}\sin\theta\right)\right]\cos^2\theta\,d\theta.$$

(Eqn. 2.12)

Recognizing that the Maclaurin expansion for

$$\ln(1+x) = x - \frac{x^2}{2} + \frac{x^3}{3} - \frac{x^4}{4} + \cdots,$$

we may expand our integral as follows:

$$f(\theta) = K\int_0^{2\pi}\ln A\,(\cos^2\theta)\,d\theta + K\int_0^{2\pi}\left[\frac{B}{A}\sin\theta - \left(\frac{B}{A}\right)^2\sin^2\theta + \left(\frac{B}{A}\right)^3\sin^3\theta - \left(\frac{B}{A}\right)^4\sin^4\theta + \cdots\right]\cos^2\theta\,d\theta.$$

(Eqn. 2.13)

$$K \ln A \int_0^{2\pi} \cos^2\theta \, d\theta = K\pi \ln A = \frac{5\pi v_*}{8\alpha} \ln A .$$

(Eqn. 2.13A)

Now the odd powers of sin θ vanish and the even powers can be integrated through the relation between the gamma and trigonometric functions (see any good textbook in Advanced Calculus) as follows:

$$\int_0^{2\pi} \cos^{s-1}x \, \sin^{n-1}x \, dx = \frac{1}{2} \frac{\Gamma(\tfrac{1}{2}s)\,\Gamma(\tfrac{1}{2}n)}{\Gamma(\tfrac{1}{2}s+\tfrac{1}{2}n)} .$$

Utilizing this relationship, and integrating term by term, we have for our integral,

$$-K\int_0^{2\pi}\left[\left(\frac{B}{A}\right)^2 \sin^2\theta\cos^2\theta + \left(\frac{B}{A}\right)^4 \sin^4\theta\cos^2\theta + \left(\frac{B}{A}\right)^6 \sin^6\theta\cos^2\theta + \cdots\right] d\theta$$

$$= -\frac{1}{2}K\left[\left(\frac{B}{A}\right)^2 \frac{\Gamma(3/2)\Gamma(3/2)}{\Gamma(3)} + \left(\frac{B}{A}\right)^4 \frac{\Gamma(3/2)\Gamma(5/2)}{\Gamma(4)} + \left(\frac{B}{A}\right)^6 \frac{\Gamma(3/2)\Gamma(7/2)}{\Gamma(5)} + \cdots\right].$$

The gamma function can be evaluated by the relationship

$$\Gamma(S+1) = S\Gamma(S) \text{ and}$$

$$\Gamma(1) = 1 \text{ and } \Gamma(\tfrac{1}{2}) = \sqrt{\pi}.$$

Therefore, our integral becomes

$$-\frac{1}{2}K\left[\left(\frac{B}{A}\right)^2 \frac{(\tfrac{1}{2}\sqrt{\pi})(\tfrac{1}{2}\sqrt{\pi})}{2} + \left(\frac{B}{A}\right)^4 \frac{(\tfrac{1}{2}\sqrt{\pi})(\tfrac{3}{4}\sqrt{\pi})}{6} + \left(\frac{B}{A}\right)^6 \frac{(\tfrac{1}{2}\sqrt{\pi})(\tfrac{15}{8}\sqrt{\pi})}{720} + \cdots\right]$$

$$= -\frac{\pi K}{16}\left[\left(\frac{B}{A}\right)^2 + \frac{1}{2}\left(\frac{B}{A}\right)^4 + \frac{1}{92}\left(\frac{B}{A}\right)^6 + \cdots\right].$$

Recombining the separate parts of Eqn. 2.11, we have, utilizing Eqn. 2. 13,

$$V_{AVE} = \frac{2.12\pi v_*}{\alpha} + \frac{5\pi v_*}{8\alpha}\ln A - \frac{5\pi v_*}{128\alpha}\left[\left(\frac{B}{A}\right)^2 + \frac{1}{2}\left(\frac{B}{A}\right)^4 + \frac{1}{92}\left(\frac{B}{A}\right)^6 + \cdots\right].$$

Remembering that $A = \frac{h}{K_s} + 0.0338$ and $B = \frac{d}{2K_s}$, we then have

$$V_{AVE} = \frac{2.12\pi v_*}{\alpha} + \frac{5\pi v_*}{8\alpha} \ln\left(\frac{h}{K_s} + 0.0338\right) - \left(\frac{5\pi v_*}{128\alpha}\right) \times \left[\left(\frac{d/2K_s}{h/K_s + 0.0338}\right)^2 + \frac{1}{2}\left(\frac{d/2K_s}{h/K_s + 0.0338}\right)^4 + \frac{1}{92}\left(\frac{d/2K_s}{h/K_s + 0.0338}\right)^6 + \cdots\right].$$

And finally we may write

$$V_{AVE} = \frac{2.12\pi v_*}{\alpha} + \frac{5\pi v_*}{8\alpha} \ln\left[\left(\frac{h}{K_s}\right) + 0.0338\right] - \left(\frac{5\pi v_*}{128\alpha}\right) \times \left[\left(\frac{d}{2h + 0.0338K_s}\right)^2 + \frac{1}{2}\left(\frac{d}{2h + 0.0338K_s}\right)^4 + \frac{1}{92}\left(\frac{d}{2h + 0.0338K_s}\right)^6 + \cdots\right].$$

(Eqn. 2.14)

Since $2h = 0.0338k_s$ will always be larger than d, the series expansion converges quite rapidly. A proof of this convergence is presented in the Appendix and a method is also given for evaluating the error term created when the series portion of Eqn. 2.14 is terminated.

Returning to Eqn. 2.7, we may write

$$F_D = \frac{1}{2} C_D \alpha_s d^2 \rho \left\{\left[\frac{2.12\pi v_*}{\alpha} + \frac{5\pi v_*}{8\alpha} \ln\left(\frac{h}{K_s} + 0.0338\right) - \left(\frac{5\pi v_*}{128\alpha}\right)\left[\left(\frac{d}{2h + 0.0338K_s}\right)^2 + \frac{1}{2}\left(\frac{d}{2h + 0.0338K_s}\right)^4 + \frac{1}{92}\left(\frac{d}{2h + 0.0338K_s}\right)^6 + \cdots\right]\right\}^2.$$

(Eqn. 2.15)

Finally, we may return to Eqn. 2.6A and write our general equation for the tractive shear stress when motion impends as follows:

$$\tau_s + \frac{C_D A \rho \beta_1 V_{AVE}^2}{2\alpha_s d^2} = \frac{\alpha}{\alpha_s} d(\gamma_s - \gamma)\beta_2,$$

and utilizing Eqn. 2.15, we have

$$\tau_s + \frac{C_D \rho \beta_1}{2}\left\{\left[\frac{2.12\pi v_*}{\alpha} + \frac{5\pi v_*}{8\alpha} \ln\left(\frac{h}{K_s} + 0.0338\right) - \left(\frac{5\pi v_*}{128\alpha}\right)\left[\left(\frac{d}{2h + 0.0338K_s}\right)^2 + \frac{1}{2}\left(\frac{d}{2h + 0.0338K_s}\right)^4 + \frac{1}{92}\left(\frac{d}{2h + 0.0338K_s}\right)^6 + \cdots\right]\right\}^2 = \frac{\alpha}{\alpha_s} d(\gamma_s - \gamma)\beta_2 \qquad \text{(Eqn. 2.16)}$$

It is admitted that Eqn. 2.16 appears to be quite formidable. However, since this is the chapter dealing with theory, the author chose to leave the solution to the tractive shear stress in its most general form. In Chapter IV - The Analysis of Results - we shall see that Eqn. 2.16 will reduce to a workable expression that can be handled with ease for the evaluation of tractive shear stresses.

CHAPTER III

TEST PROCEDURE

Plan of Experiments

It was originally planned to use essentially the same test procedure as was used by Laursen and Hwang (op. cit.) and by Harp (op. cit.) except that the Preston calibration procedure would be eliminated from the process. It is felt that this simplification was justified, since, in both tests, it had been adequately demonstrated that Preston's pressure-shear stress relationship magnitudes had remained valid through the entire range from laminar through the rough range of flow.

Description of Equipment

The system was composed of a sump, pumps, piping and a flume with varying cross-section and a discharge system which returned the flow to the sump so that the system was self contained. Instrumentation included a pitot tube, pressure converter, pressure transducer, electronic preamplifier, galvanometer and recorder unit.

The sump is 30 feet long, 15 feet wide and 7½ feet deep. It is concrete lined and covered so that the water remained clean during the entire test period.

A Worthington centrifugal pump driven by a variable speed General Electric motor was used.

The flow rate was metered by a 1.654 inch bore, flat orifice plate and water and mercury manometers. The piping was 2 inch I.D. steel pipe.

The orifice plate was calibrated by using a weigh tank and stop watch. Calibration curves for both the water and mercury manometers are included in this report as Fig. 10 and Fig. 11 in the Appendix.

Water was admitted to the flume through a vertical down-pipe resting on the bottom of the flume. Turbulence and shock were minimized by drilling numerous holes in the down-pipe so that water entered the forebay radially over a 360° arc and through the complete depth of the flume. In addition, 150 copper tubes four inches long and ½ inch in diameter were stacked in the flume to further reduce turbulence and to direct the flow. The turbulence reduction scheme proved quite effective. There was almost no surface waviness and buoyant material admitted to test for total turbulence was found to traverse the entire flume length in virtually a straight line.

The flume itself was constructed of ¼ inch plexiglass. It was nine feet long and 18 inches high. The forebay was one foot wide and three feet long. The working section was six feet long. It tapered in width from one foot just downstream from the forebay, to 1½ inches in width at the discharge end. A schematic view of the flume with leading dimensions is shown as Fig. 3 of this report, and photographically as Fig. 4. The discharge was received in a cylindrical receptacle and was returned to the sump.

As originally planned, the pitot tube was made of two long veterinarian hypodermic needles having an inside diameter of 0.023 inch and an

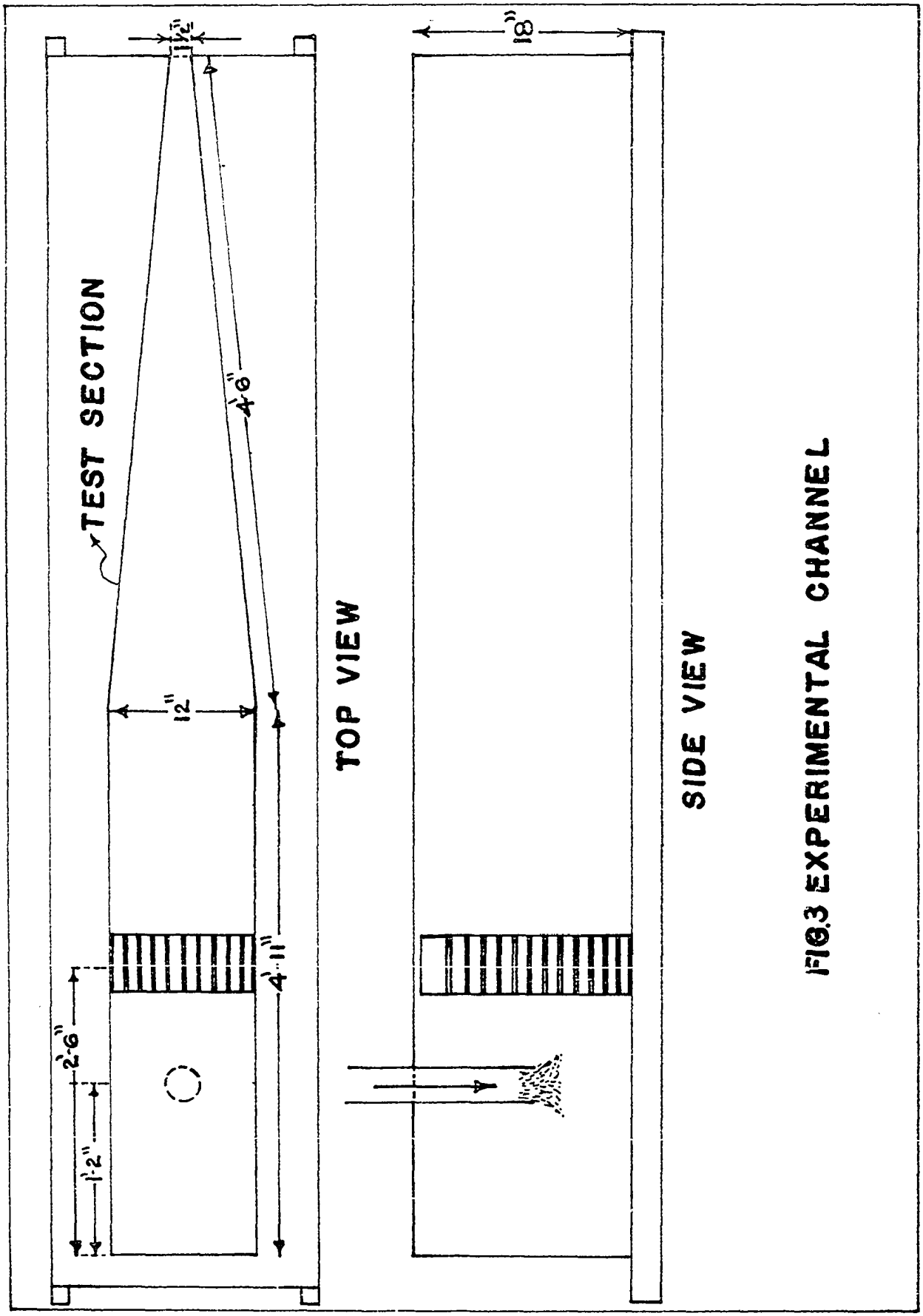

FIG.3 EXPERIMENTAL CHANNEL

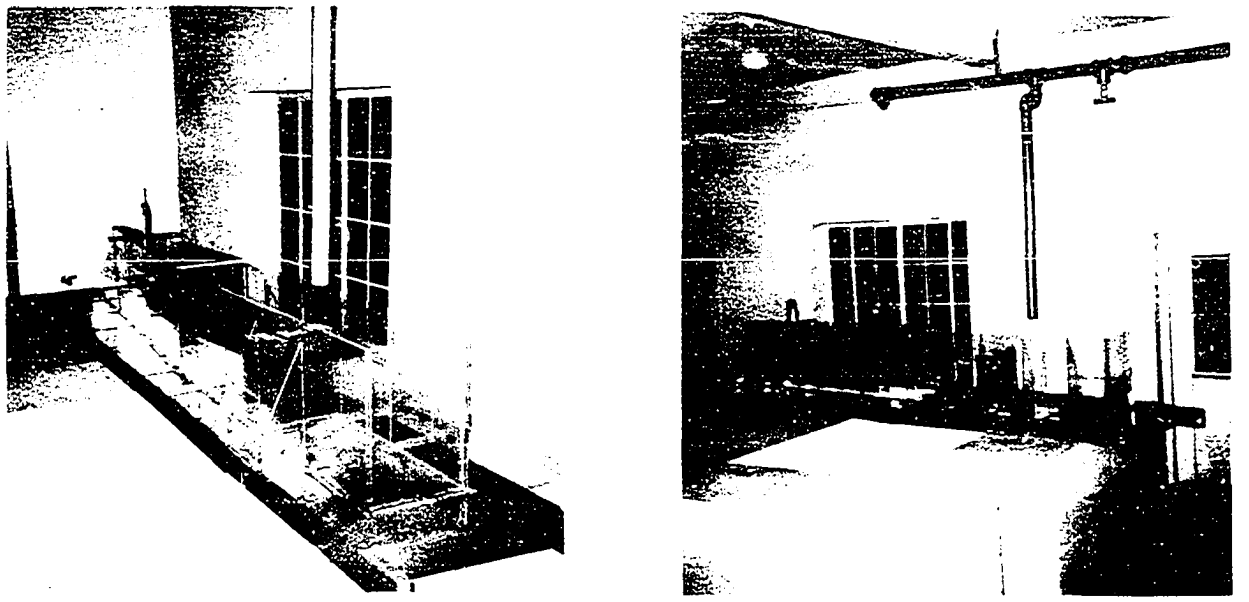

Fig. 4. The Experimental Channel

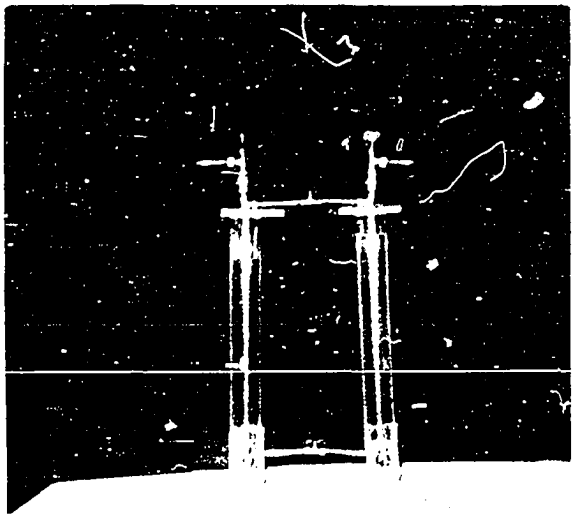

Fig. 5. The Pressure Converter

outside diameter of 0.035 inch. The pitot tubes led to a pressure converter by 1/8 inch tygon tubing.

Both Laursen and Hwang and Harp had felt that since pressure transducers were sensitive to air pressure differences and since they were measuring water pressure differences, that it was necessary to include in the system a method of converting water pressure to air pressure. They both accomplished this by constructing two plastic cylinders which were valved and interconnected in such a manner that each tube could be vented to the atmosphere and both tubes could be adjusted to the same internal pressure. This same scheme was adopted for this project. A photograph of this pressure converter is shown as Fig. 5 of this report.

The pressure differential was measured by a Statham temperature compensated pressure transducer with a pressure range of $\pm$ 1 psid and compensated temperature interval of -65°F to + 250°F. The manufacturers calibration factor of 2668 microvolts (open circuit) per volt per psi was used in performing all tests.

The transducer output signal was received by a Sanborn Carrier Preamplifier model 350-1100B which fed this signal to a Sanborn two-channel recording system, model 296, and simultaneously to a Sanborn model 760-20 galvanometer. It was found that the galvanometer was much more convenient to use during tests than was the recorder. The preamplifier and galvanometer are shown as Fig. 6 of this report.

It should be mentioned in passing that a micromanometer could have been used to measure the pressure differential. However, this idea was not seriously pursued since the factory-calibrated pressure transducer,

preamplifier unit and galvanometer had just recently been purchased and were available for use on this project.

Cohesionless Material Characteristics

At the outset of this project it was decided to investigate the behavior of cohesionless materials of different specific gravities and of different grain-sizes.

The materials selected for use were a bank-run, washed quartz course sand and gravel obtained locally and course gypsum sand obtained from the White Sands National Monument, New Mexico.

The course sands and gravel were oven dried and sieved mechanically in a gyratory shaker. The size increments were chosen arbitrarily as passing No. 3/8 and retained on No. 4. Passing No. 4 and retained on No. 10. Passing No. 10 and retained on No. 20. Passing No. 20 and retained on No. 40. Sieve sizes are for U. S. Standard sieves with square mesh openings.

It is felt that these arbitrary gradations are logical. Material larger than No. 3/8 would require discharges beyond laboratory capabilities, and sizes smaller than No. 40 were so small that it was difficult to detect the point where grain movement began.

After the sand and gravel had been graded, representative samples were withdrawn from each fraction and the standard (ASTM D 854) soil mechanics laboratory specific gravity test was performed on each fraction.

Originally, a portion of each grain-size was dyed with vegetable dye. It was planned to use the dyed grains as the topmost layer for each run, so that it would be easier to detect the zones of grain movement.

After several runs it became evident that this was an unnecessary step. By careful observation, it was possible to detect the places of movement with little or no difficulty. As a consequence, the colored sand was not used on most of the runs.

Christensen (op. cit.) has shown analytically that for uniform sand, the most probable average size is the D_{50} size. This would not be true for well-graded soil where the relation

$$d_{AVE} = \sqrt{d_{MAX}\, d_{MIN}}$$

would have to apply. However, for uniform soil, it can be seen that the arithmatic and geometric averages are about equal. That is, the mean of the maximum and minimum size may be used as the representative size of the fraction.

In Table I are given the pertinent characteristics of the materials used in these tests.

TABLE I

BED-MATERIAL CHARACTERISTICS

Sieve No.	Grain Dia-In	Specific Gravity of Solids	Grain Shape	Ave Ks ft=D_{35}
		Quartz Sand and Gravel		
3/8"	0.375			
			spherical	0.0235
4	0.187	2.63		
			spherical	0.01108
10	0.0787	2.63		
			spherical	0.004243
20	0.0231	2.63		
			spherical	0.001647
40	0.0164	2.63		
		Gypsum Sand		
10	0.0787			
		2.29	rice-shaped	0.004243
20	0.0231			
		2.29	rice-shaped	0.001647
40	0.0164			

There was no fraction of the gypsum sand larger than the No. 10 sieve size.

A layer of number 10 quartz sand was glued to the flume bottom as a permanent layer. This was done to provide sufficient roughness to prevent the sand bed as a whole from sliding downstream under the action of the water.

After 18 tests had been run under the above described scheme, it was decided that the system was not functioning properly. Testing was suspended and the components of the system were analyzed to try to detect what was wrong. The following conclusions were reached:

a) The pitot tube openings were too small. Capillary tension produced by the very small diameter tubes produced forces which overpowered the very small pressure differences being measured.

b) The time delay while the pressure converter was reacting was unacceptable, and the reliability of the pressure conversion from water pressure to air pressure was very questionable.

It was decided to make another pitot tube with sufficiently large bore that capillary tension forces would not be established. This was done. The new pitot tube was constructed of stainless steel tubing having 1/8 inch O.D. and 1/16 inch I.D. The wall thickness was 1/32 inch. This pitot tube is shown as Fig. 7 of this report.

It was decided to see if the pressure transducer could be operated without a pressure converter. The transducer was placed at a sufficient elevation above the top of the flume so that there was no chance of water being forced up the pitot tube leads into the transducer. A trial run showed that this scheme worked beautifully. There was almost instantaneous response to all pressure changes and there was no drift due to capillary forces building-up.

After the new pitot tube was made and the pressure converter was eliminated from the system, no further changes were made during the experimental phase of this project.

Test Procedure

Before each test run, the flume was prepared by sprinkling a level bed approximately one inch thick of the selected gradation of sand onto the bottom of the flume. Christensen had shown analytically that the

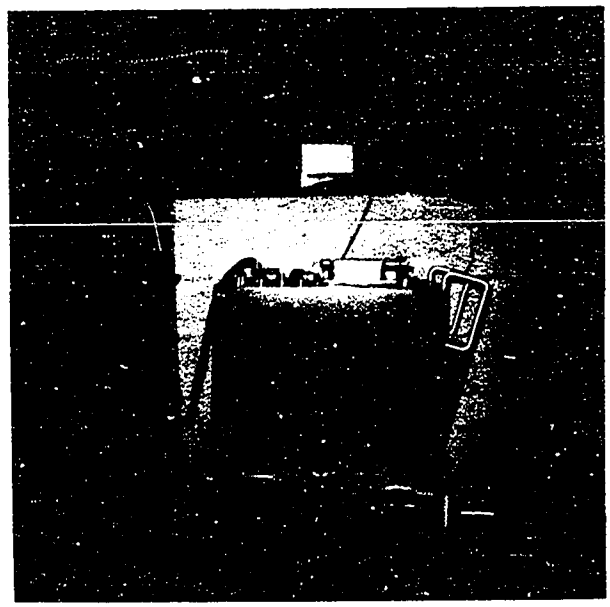

Fig. 6. Preamplifier Unit and Galvanometer

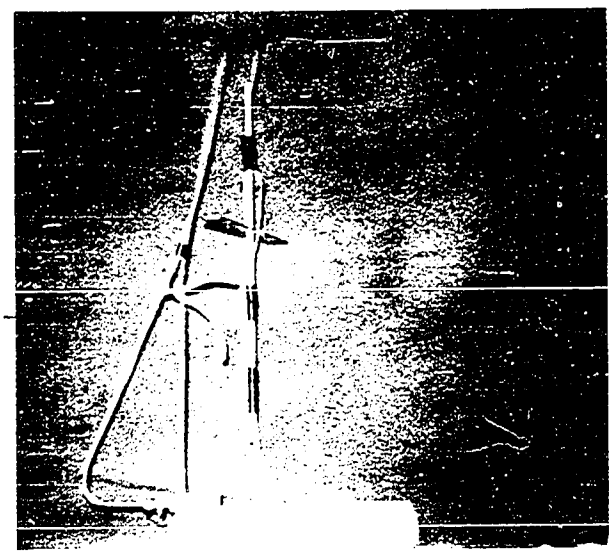

Fig. 7. The Pitot Tube and Pressure Transducer

shear stress required to cause bed movement was independent of the void ratio of the bed material. In addition, he studied the influence of stacking configurations and was still satisfied with this conclusion. Therefore the bed was always prepared in a loose, sprinkled state. The preamplifier was balanced and the test was started.

Each run was started at minimum discharge and the discharge increased after each reading. The first reading for each run was taken with the grains in the laminar or transitional range, then all succeeding readings taken with the grains in the rough range. This change of regime was fairly easy to detect. When the flow was laminar or transitional, the read-out would be about half the value of the read-out in the rough regime. It does not take an operator very long to learn to predict the regime by the magnitude of the read-out.

At each increment of discharge, the flume bed was carefully watched for bed movement. As soon as movement was detected, it was watched while it travelled upstream until it stabilized itself at some distance from the outfall. When stabilization occurred, the pitot tube was lowered into the flume and positioned parallel to the longitudinal axis of the flume and just touching the bed. It was positioned in such a manner that the dynamic port was just upstream from the point of stabilized movement. When the pitot tube was positioned, the preamplifier read-out was recorded from the galvanometer, and the pitot tube distance from the outfall was recorded as well as the water depth at the point of stabilized motion. The manometers were read and the discharge again increased at which time the entire cycle was repeated.

The discharge was incrementally increased until maximum pump capacity was obtained. By this time instability of the bed had progressed a considerable distance upstream and the downstream bed had almost completely eroded away.

After maximum discharge was reached, the water was turned off and the bed re-fixed for the next run.

Runs were continued on the same fraction of sand until the investigator was convinced that the readings were consistent and were being reproduced run after run. This usually occurred somewhere between the fifth and tenth run.

After it was determined that the readings were being reproduced reliably, the bed was cleared of the old fraction and a new fraction was placed in the bed.

CHAPTER IV

ANALYSIS OF RESULTS

Simplification of the General Expression

In Chapter II, a quite formidable general expression was developed for the tractive shear stress when motion impends on a sand particle. It was pointed out at that time that this expression would reduce to a workable form.

First, let us examine the general expression for the average velocity, Eqn. 2.14. Christensen (op. cit.) has shown that h most logically may be taken as 0.718d and that $k_s = d$. Substituting these relationships into Eqn. 2.14 and evaluating, we find that Eqn. 2.14 reduces to the form

$$V_{ave} = 7.67 v_*. \qquad \text{(Eqn. 2.14a)}$$

Now we may rewrite Eqn. 2.16 as follows:

$$\tau_s + \frac{C_D \rho \beta_1 (7.67 v_*)^2}{2} = \frac{\alpha}{\alpha_s} d(\gamma_s - \gamma)\beta_2. \qquad \text{(Eqn. 2.16a)}$$

Experimental investigations by Dalton and Masch (4.1) have shown that within the range of our investigations, the drag coefficient, C_D, may be evaluated as ranging between 1.1 and 1.4. Morris (4.2) suggested that C_D for spheres be taken as 1.2 and for elliptical (rice-shaped) grains that 0.5 be used.

For our quartz sand let us take $C_D = 1.2$ and further reduce Eqn. 2.16.

$$\tau_s + 35.28\rho\beta_1(v_*)^2 = \frac{\alpha}{\alpha_s} d(\gamma_s - \gamma)\beta_2 .$$

(Eqn. 2.16b)

Recognizing that

$$v_* = \sqrt{\tau_o/\rho},$$

we may still further simplify Eqn. 2.16. In addition, when motion impends, τ_s becomes τ_o, and we may write

$$\tau_o + 35.28\beta_1\tau_o = \frac{\alpha}{\alpha_s} d(\gamma_s - \gamma)\beta_2 .$$

Solving for τ_o, we have

$$\tau_o = \frac{\alpha}{\alpha_s} d \frac{(\gamma_s - \gamma)\beta_2}{(1 + 35.28\beta_1)} = d(\gamma_s - \gamma)\beta_3,$$

(Eqn. 4.1)

where

$$\beta_3 = \frac{\alpha}{\alpha_s} \frac{\beta_2}{(1 + 35.28\beta_1)}$$

In its expanded form, we may write

$$\beta_3 = \frac{2}{3} \frac{(l_w + l_A)}{(36.28 l_A \cot\theta + l_s + 35.28 l_D)} .$$

Referring again to Fig. 1 we may assign logical values to the various moment arms. We know that $0 \leq l_w \leq \frac{d}{2}$ let us assign a value of $l_w = \frac{2d}{5}$. We know $-\frac{d}{2} \leq l_A \leq \frac{d}{2}$; let us assign it a value of $-\frac{d}{3}$. We know that both l_D and l_s are $\geq \frac{d}{2}$. For these two values, let us assign $\frac{3d}{5}$. If the grains were perfect spheres, θ would be exactly 30°. Let us use this value.

Substituting these values, we obtain

$$\beta_3 = 0.182.$$

An evaluation of the critical shearing stress for the four sizes of quartz sand, and for the two sizes of gypsum sand is shown graphically as Fig. 8 of this report, and in tabular form as Table II.

TABLE II

THEORETICAL AND EXPERIMENTAL CRITICAL

SHEARING STRESSES

Grain Size ft	Mullis Theoretical τ_o -psf	Mullis Experimental τ_o -psf	Harp Experimental τ_o -psf	White Experimental τ_o -psf
		QUARTZ SAND		
0.0235	0.434	0.2285	0.167	0.263
0.01108	0.202	0.190	0.088	0.135
0.004243	0.0783	0.104	0.038	0.056
0.001647	0.0304	0.054	0.015	0.025
		GYPSUM SAND		
0.004243	0.062	0.110	0.030	0.045
0.001647	0.0241	0.0555	0.012	0.020

An inspection of Fig. 8 will reveal that the experimental and theoretical shear stresses agree quite well for the middle ranges of grain sizes, but tend to deviate for the extreme sizes at both ends of the range.

There is a logical explanation for this occurrence. It was found that β_3 is extremely sensitive to small changes in the values of the various moment arms. In addition, since the grains are not perfect spheres, it may be assumed that θ is not a constant 30°.

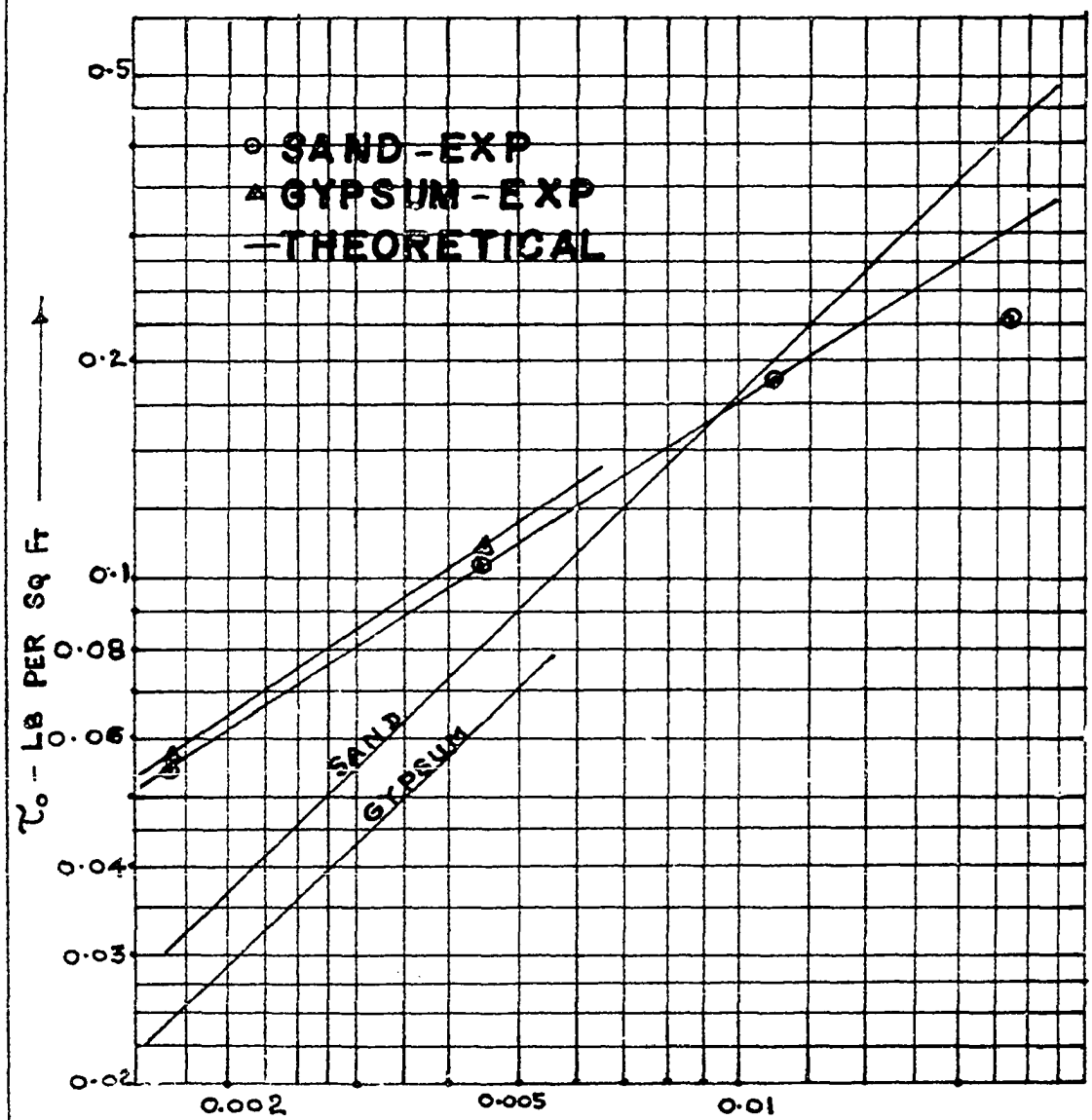

FIG.8 THEORETICAL AND EXPERIMENTAL SHEARING STRESSES

Comparison with Shields' Diagram

In Fig. 9 of this report is shown the "classical" Shields' diagram with the results of White (op. cit.), Harp (op. cit.) and the author superimposed. After an inspection of this diagram, several items will be noted:

1) The data of all investigators except Harp's turbulent values plot well above Shields' values.
2) All data, including Shields', tend to converge at high values of d/δ'.
3) All data tend to slope down and to the right rather than "sag" as Shields indicates that it should.
4) All data, except Shields', tend to plot as straight lines.

There has never been a good explanation for the definite "sag" in Shields' diagram. However, as was pointed out in Chapter I of this report, Shields assumed that no analytical solution to the problem was possible. He made gross assumptions, took data, and changed his assumptions as necessary to fit his conclusions.

Comparison with White's Data

White made no attempt to draw curves through his data. He merely plotted them on the Shields' diagram. It would be very difficult to attempt to duplicate his results since he arbitrarily specified "general bed movement," "1% movement of top grains," and "very few grains move." These specifications would depend completely on the experimentors' judgment. Even with these limitations, White's data exhibited the downward slope to the right and plotted above the Shields' diagram. In addition, White's

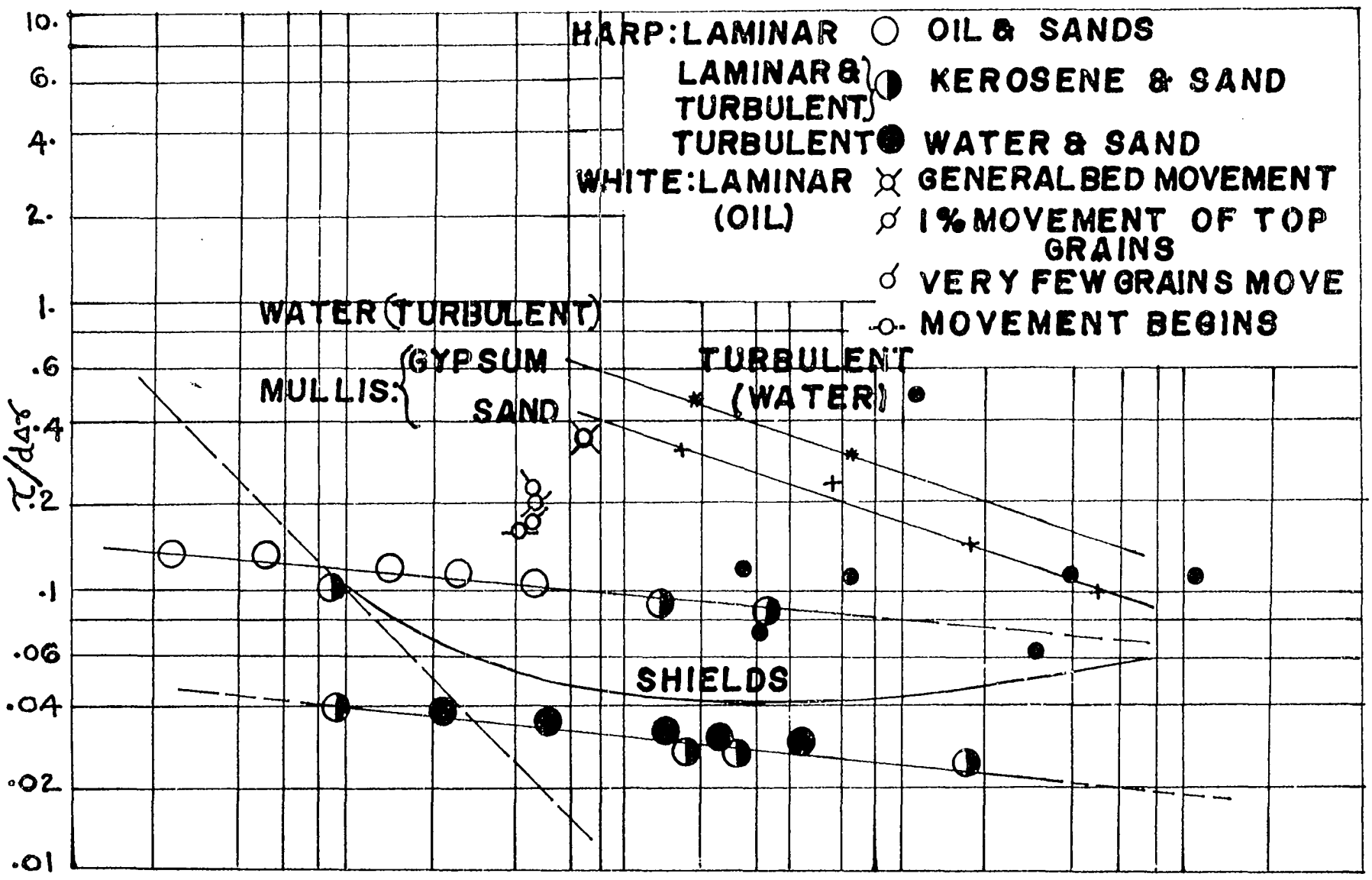

FIG. 9 SHIELDS' DIAGRAM

values tend to converge with all other data at large values of d/δ'.

Comparison with Harp's Data

Harp did draw curves through his data and the curves did exhibit the down slope to the right. Harp's turbulent values were the only ones of all the investigators that plotted below the Shields' diagram. The only explanation for this that the author can present, is that Harp's instrumentation could have been improperly calibrated or that Harp's tests were conducted in the transition range instead of in the turbulent range as he thought.

Experimental Equations

It has previously been shown, Eqn. 4.1, that the theoretical evaluation for the critical shear stress is

$$\tau_o = d(\gamma_s - \gamma)/\beta_3 .$$

This is exactly the same form that White used. He gave his evaluation as

$$\tau_o = K d(\gamma_s - \gamma).$$

The equations for the experimental values of Harp's two curves are

$$\tau_o = d(\gamma_s - \gamma)(0.095)(d/\delta')^{0.085} \qquad \text{(Eqn. 4.2)}$$

for his laminar tests, and

$$\tau_o = d(\gamma_s - \gamma)(0.032)(d/\delta')^{0.104} \qquad \text{(Eqn. 4.3)}$$

for his turbulent values.

Since the authors curves for the two types of sand were exactly parallel, they differed only by a constant. The equation for the quartz sand is

$$\tau_o = d(\gamma_s - \gamma)(0.38)(d/\delta')^{0.33} \qquad \text{(Eqn. 4.4)}$$

and for the gypsum sand is

$$\tau_o = d(\gamma_s - \gamma)(0.55)(d/\delta')^{0.33}. \qquad \text{(Eqn. 4.5)}$$

The term, $(d/\delta')^K$ is not the constant that theory tells us it should be. It is noted that the exponent, k, is very small for both of Harp's curves and small for both the author's curves. If k were extremely small, or most desirably equal to zero, then $(d/\delta')^K$ would be equal to one, and the desired theoretical result would be exactly duplicated experimentally. Unfortunately, this is not the case. Obviously the term $(d/\delta')^K$ has an influence on the problem that is not at all understood at the present development state of the theory.

It is suspected that there exists some factor involving the influence or slope of the energy grade line that is not expressed in the theoretical development. This aspect is worthy of further detailed study.

CHAPTER V

DISCUSSION, CONCLUSIONS AND RECOMMENDATIONS

Discussion

Based upon the theoretical and experimental results of this project, the following conclusions are presented:

1) The Preston shear technique is well adapted for the laboratory measurement of critical tractive shear stresses on cohesionless bed material.

2) It is imperative that all electronic equipment be in first-class working order and properly calibrated before and during all laboratory test work. The importance of good quality, properly calibrated electronic equipment cannot be over-emphasized. Since most civil engineers only understand in a general manner the internal workings of their electronic equipment, they are usually unable to judge whether voltage read-outs and other electronic evaluations are subject to non-hydraulic effects or not. Furthermore, they do not usually know what normal, and natural variations may be expected from the equipment. Therefore, only if it is known that the equipment is properly adjusted and calibrated, can they accept electronic read-outs with confidence, and accept variations as being solely due to hydraulic variations.

3) It is essential that the pitot tube have a sufficiently large bore. This is necessary to prevent the formation of extraneous capillary tension forces which are capable of completely disguising the very small changes in pressure that are being measured. It is also desirable for mechanical operating purposes to construct the pitot tube with as small a wall thickness as available material will permit.

4) The use of the Shields' diagram as the standard basis of comparison is simply not justifiable. The "sag" shape does not correlate with three independent investigations. Since Shields' work was extrapolated from the bed-load transport curve to the time that bed-load ceases, his procedure could easily yield values that were erratic due to the very nature of the bed-load transport curve. In addition, the axes of the Shields' diagram are $\tau_o/(d\gamma)$ and d/δ'. While these parameters are dimensionless and seemingly correct, it should be noted that one actually plots τ_o against τ_o.

5) It is very difficult to try to correlate laboratory results with those of White. As has been pointed out, White plotted values obtained under the conditions of "general bed movement," "1% movement of top grains," "very few grains move," etc.

6) Christensen's velocity distribution formulae yield valid

results at and near the boundary. In addition, his velocity relationships are the only ones known to have this property.

7) The constant term, β_3, appearing in Eqn. 4.1, is extremely sensitive to very small changes in moment arm values.

8) The angle of inclination, θ, of the normal force to the vertical theoretically should be a constant, and for uniform grain-sizes, should be equal to 30°. However, it is felt that this is not true, particularly if the grain-size deviates appreciably from uniform, and/or if the grain-shape deviates appreciably from spherical.

Conclusions

A theoretical formula has been developed which describes the critical tractive shear stress developed on cohesionless bed material in the rough range of flow. This theoretical value compares qualitatively with experimental results. The maximum deviation between experimental values and theoretical values of τ was 0.2 psf over a range of grain sizes of 0.0235 ft to 0.001647 ft and this maximum deviation occurred at the end point where d equals 0.0235 ft.

Recommendations

As an aid to future investigators, the following recommendations are presented, which it is hoped, will smooth their work and also suggest areas in which much more work is needed before we can fully understand the total problem of critical tractive shear stresses.

1) A much better method of evaluating the moment arms associated with the various forces in the problem is needed.

2) Work needs to be done on determining if and how the angle θ varies, and if it is found that it does, in fact, vary; then some method of determing this value is needed.

3) The problem of determining exactly where the critical tractive shearing stress actually occurs has never been properly defined. At present it is an "engineers judgment" type problem and it is suspected that no two investigators would select exactly the same place to measure this phenomenon.

4) All published work to date has been done in channels with flat beds. It is suggested that work be done utilizing channels with slopes. Christensen has done some theoretical evaluation in this area.

5) All previous investigators have attempted to eliminate or greatly reduce both local and gross turbulence. It is suggested that the influence of both local and gross turbulence be studied both analytically and experimentally.

6) No published studies of the influence of dunes and ripples on the problem is known. This is another area that needs investigation.

7) In all studies to date, the investigators have used very uniform cohesionless bed-material. Work needs to be done using well-graded cohesionless bed-material. Any studies in which cohesive bed-materials are utilized would, indeed be formidable, and perhaps impossible to accomplish, but, of course, this work will ultimately have to be done before we can have a complete understanding of the problem.

Summary

Over the years much progress has been made in understanding the phenomenon of critical tractive shear stresses. The door was really opened in the 1950's with the development of Preston's shear technique.

Methods have now been developed for the analytical evaluation of the velocity distribution at and near the boundary.

A theoretical evaluation of critical tractive shear stresses has been presented. Laboratory measurements of these stresses were made utilizing the Preston technique. A comparison of theoretical and experimental values was made and fairly good agreement was obtained. The maximum deviation of experimental values of τ_o from the theoretical values was 0.2 psf over the range $0.0235 \geq d \geq 0.001647$ ft. This maximum deviation occurred at the end point where d equals 0.0235 ft.

The experimental values obtained were compared with the results of other investigators who had used similar and very different laboratory techniques. The qualitative comparison was quite acceptable. Over the

range of $2 \leq d/\delta' \leq 60$, the maximum deviation of the experimental values of $\tau_o/d\gamma$ obtained in this project with those obtained by Harp was 0.4 occurring at the end point where d/δ' equals 2. The maximum deviation of the values obtained in this project with those obtained by White was 0.3 occurring at the end point where d/δ' equals 2.

BIBLIOGRAPHY

Specific References

(1.1) Leliavsky, Serge, An Introduction to Fluvial Hydraulics. London: 1955.

(1.2) Lacey, G., "Stable Channels in Alluvium," Min. Proc. Inst. Civ. Eng., Vol. 229, 1930.

(1.3) DuBuat, L. G., Principes d'Hydrauliques. Paris: 1816.

(1.4) Inglis, Sir Claud, "Historical Note on Empirical Equations," I. A. H. R., 2nd Meeting. Stockholm: 1948.

(1.5) Straub, L. G., House Document 238. 73rd Congress. U. S. Government Printing Office. Washington, D. C. 1935.

(1.6) Lane, E. W., "Design of Stable Channels," Trans. A. S. C. E., Vol. 120, 1955.

(1.7) Shields, A., "Anwendung der Aeknlichkeitsmechanik und der Turbulenz-Forschung auf die Geschiebewegung," Mitteilungen der Preuss. Versuchsanst. f. Wasserbau u. Schiffbau., Berlin, Heft 26, 1936.

(1.8) White, C. M., "Equillibrium of Grains on Bed of Stream," Proceedings Royal Society of London, Vol. 174A, 1940.

(1.9) Christensen, Bent A., "A Treatise on the Critical Shear Stress in Alluvial Watercourses." Unpublished Ph.D. dissertation, University of Minnesota, 1961.

(1.10) Preston, J. H., "The Determination of Turbulent Skin Friction By Pitot Tubes," Journal of Royal Aeronautical Society 110, Vol. 58, 1954.

(1.11) Hsu, E. Y., "The Measurement of Local Turbulent Skin Friction By Means of Surface Pitot Tubes," David W. Taylor Model Basin Research and Development Report No. 957, 1955.

(1.12) Laursen, E. M., and Hwang, L. S., "Extension of Preston"s Shear Measurement Technique to Rough Boundaries," Technical Report No.1, NSF G-7409, National Science Foundation, 1962.

(1.13) Harp, J. F., "Critical Tractive Force of Uniform Sands." Unpublished Ph.D. dissertation, University of Arizona, 1963.

(4.1) Dalton, C. and Masch, F. D., "The Influence of Secondary Flows on Drag Forces," Tech. Rep. HYD 04-6503, The University of Texas, 1965.

(4.2) Morris, H. M., Applied Hydraulics in Engineering. New York: The Ronald Press, 1963.

General References

Hildebrand, F. B., Advanced Calculus For Application. New Jersey: Prentice-Hall Inc., 1948.

Brand, L., Advanced Calculus. New York: John Wiley and Sons, 1955.

Engineering Hydraulics. Edited by Hunter Rouse. New York: John Wiley and Sons, 1950.

Rouse, Hunter and Howe, J. W., Basic Mechanics of Fluids, New York: John Wiley and Sons, 1953.

Chow, Ven T., Open-Channel Hydraulics. New York: McGraw-Hill, 1959.

Linsley, R. K., Jr., Kohler, M.A., and Paulhus, J. L. H.. Applied Hydrology. New York: McGraw-Hill, 1949.

APPENDIX I

Calibration Curves and Experimental Data

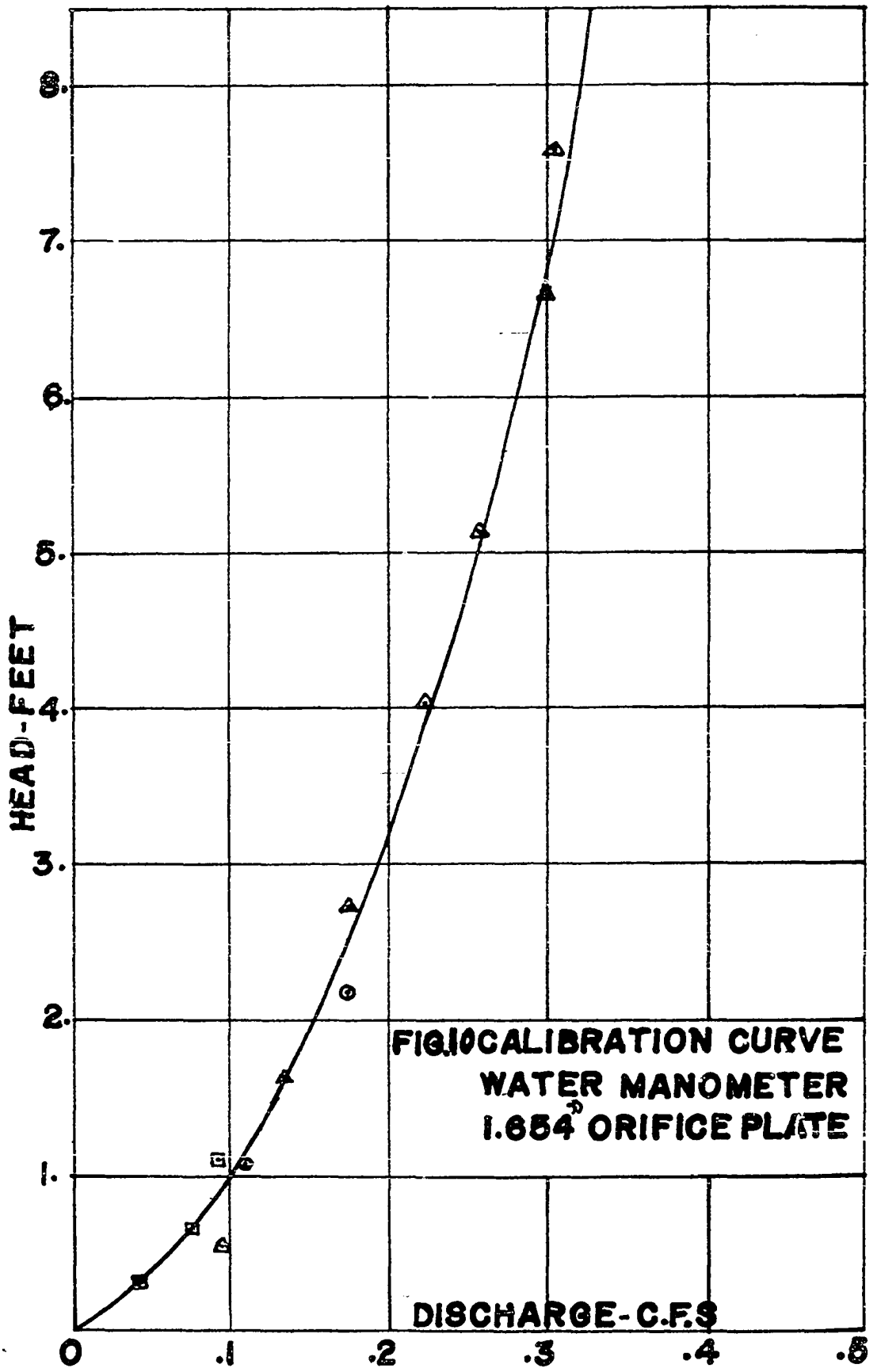

FIG.10 CALIBRATION CURVE
WATER MANOMETER
1.654" ORIFICE PLATE

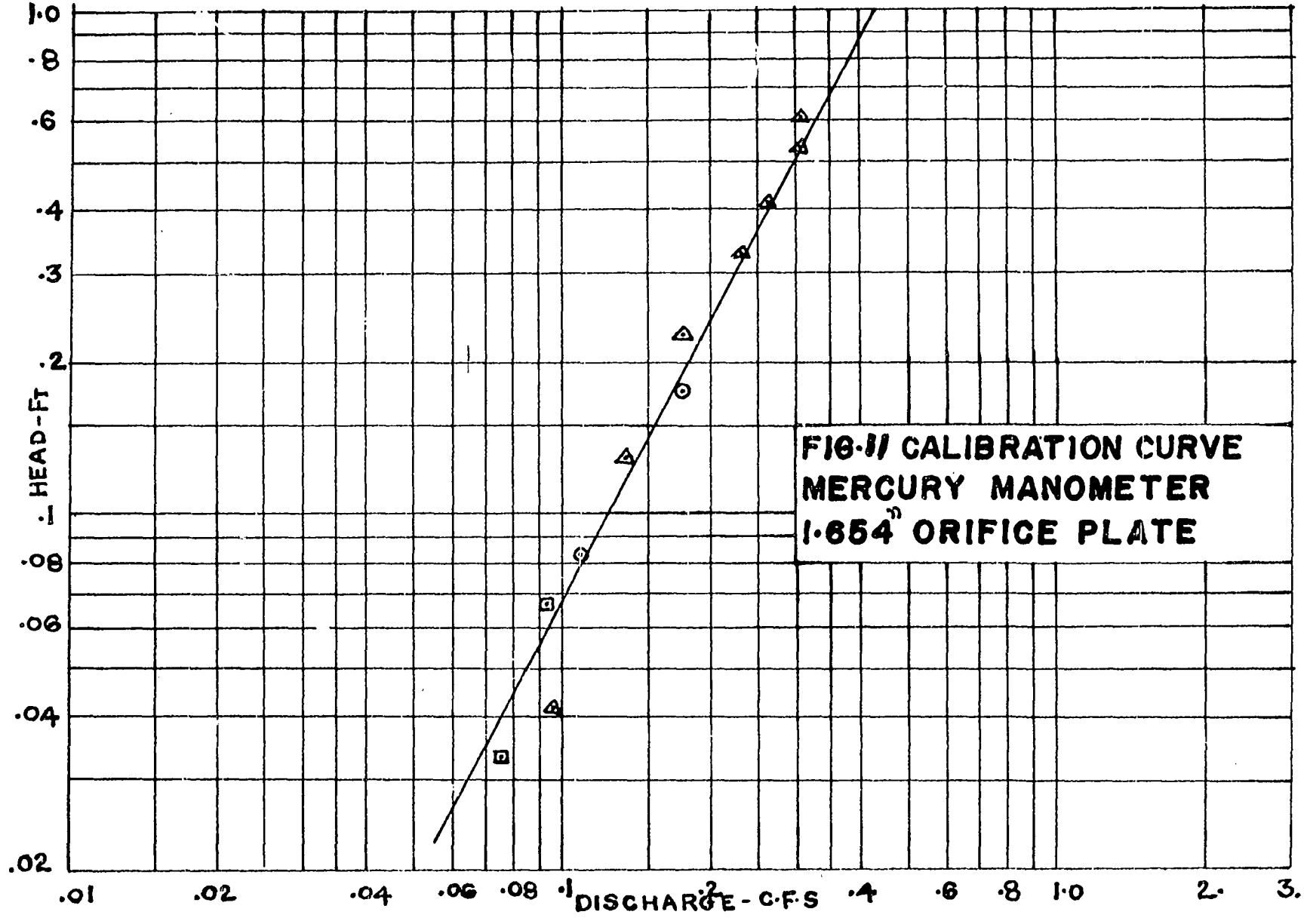
1.0
.8
.6
.4
.3
.2
.1
.08
.06
.04
.02
HEAD-Ft
.01
.02
.04
.06
.08
.1
.2
.4
.6
.8
1.0
2.
3.
DISCHARGE - C.F.S
FIG. II CALIBRATION CURVE
MERCURY MANOMETER
1.654" ORIFICE PLATE

TABLE III

EXPERIMENTAL DATA

Run No.	Water Temp °F	Discharge, Q, cfs	Velocity, Vcr, ft/sec	Pitot Tube Δp, $lb/in^2 \times 10^{-3}$
	No. 4 Quartz Sand - $k_s = 0.0235$ ft = d.			
1	49	0.393	1.45	3.52
2	49	0.544	1.65	3.30
3	49	0.269	1.35	2.30
4	49	0.315	1.46	2.80
5	49	0.351	1.43	3.50
6	49	0.336	1.62	3.44
	No. 10 Quartz Sand - $k_s = 0.001108$ ft = d.			
7	44	0.260	1.44	3.64
8	44	0.364	1.38	3.10
9	45	0.221	1.10	3.02
10	45	0.265	1.27	3.26
11	46	0.218	1.13	2.88
	No. 20 Quartz Sand - $k_s = 0.004243$ ft = d.			
12	44	0.238	0.91	2.17
13	51	0.223	0.77	4.50
14	52	0.227	0.89	2.84
15	46	0.246	0.83	3.08
16	42	0.238	0.86	2.59
17	42	0.237	0.87	3.10
18	43	0.248	0.90	2.78
19	43	0.248	0.93	1.95
20	49	0.216	0.83	2.78

TABLE III - continued

Run No.	Water Temp °F	Discharge, Q, cfs	Velocity, Vcr, ft/sec	Pitot Tube Δp, lb/in^2 x 10^{-3}
		No. 20 Gypsum Sand - k_s = 0.004243 ft = d.		
21	51	0.253	0.85	3.00
22	52	0.242	0.88	2.54
23	52	0.257	0.75	3.12
24	53	0.209	0.85	2.68
25	53	0.246	0.69	3.38
26	53	0.229	0.81	3.10
		No. 40 Quartz Sand - k_s = 0.001647 = d.		
27	50	0.217	0.85	2.78
28	50	0.249	0.77	3.32
29	50	0.252	0.80	2.12
30	50	0.215	0.83	2.88
31	51	0.224	0.85	2.88
32	51	0.222	0.83	2.80
33	51	0.275	0.80	3.16
		No. 40 Gypsum Sand - k_s = 0.001647 = d.		
34	52	0.221	0.84	2.62
35	52	0.210	0.81	2.60
36	52	0.210	0.84	3.04
37	52	0.186	0.73	2.48
38	52	0.205	0.82	3.14
39	52	0.233	0.84	2.92
40	52	0.233	0.80	3.18

TABLE IV

EXPERIMENTAL DATA (IN SHIELDS' DIAGRAM FORM)

Sand Size, ft	Sand Type	τ_o, psf	$\tau_o/d\Delta\gamma$	$\tau_o/d\Delta\gamma$
0.0235	Quartz	0.233	0.0976	49.1
0.01108	Quartz	0.190	0.169	18.8
0.004243	Quartz	0.104	0.2415	5.41
0.001647	Quartz	0.054	0.322	1.685
0.004243	Gypsum	0.11	0.322	6.375
0.001647	Gypsum	0.0555	0.418	1.76

APPENDIX II

A Proof of The Convergence of The Series Terms of Equation 2.14

A PROOF OF THE CONVERGENCE OF THE SERIES TERMS OF EQUATION 2.14

The series terms of Eqn. 2.14 are:

$$\left[\left(\frac{d}{2h+0.0338K_s}\right)^2+\frac{1}{2}\left(\frac{d}{2h+0.0338K_s}\right)^4+\frac{1}{92}\left(\frac{d}{2h+0.0338K_s}\right)^6+\cdots\right].$$

Since $2h + 0.0338K_s$ will always be larger than d, the series expansion converges quite rapidly. This can be shown as follows. Let

$$\left(\frac{d}{2h+0.0338K_s}\right)^2 = r < 1.$$

Then the series can be written

$$T=\sum_{i=1}^{\infty} K_i r^i,$$

where K_i = coefficient developed in the gamma solution, and $K_i < 1$.

Now the geometric series may be written

$$S=\sum_{i=1}^{\infty} r^i,$$

where each $r^i < 1$.

The geometric series is a standard convergent series, and upon term-by-term comparison with our series, it is seen that the geometric series dominates our series. Therefore, our series converges by comparison.

APPENDIX III

A Method of Calculating The Number of Terms Required in The Series to Produce An Error Term That Is Less Than Any Assigned Error

A METHOD OF CALCULATING THE NUMBER OF TERMS REQUIRED IN THE SERIES TO PRODUCE AN ERROR TERM THAT IS LESS THAN ANY ASSIGNED ERROR

Any user of Eqn. 2.14 would be interested in knowing how many terms of the infinite series are required to keep the error produced by termination within acceptable limits. The number of terms may be calculated as follows:

Rewriting the geometric series, we have

$$S = r^1 + r^2 + \cdots + r^n + \sum_{i=n+1}^{\infty} r^i ,$$

where

$$\sum_{i=n+1}^{\infty} r^i = R_s ,$$

the remainder after n terms. This remainder may be written

$$R_s = r^n \left(\frac{r}{1-r}\right).$$

Rewriting our series, we have

$$T = K_1 r^1 + K_2 r^2 + \cdots + K_n r^n + \sum_{i=n+1}^{\infty} K_i r^i ,$$

where

$$\sum_{i=n+1}^{\infty} K_i r^i = R_T ,$$

the remainder after n terms.

Now $R_T \leq R_s$ since

$$K_i r^i \leq r^i \quad \text{for all } i, \text{ and } R_s - R_T > 0.$$

Since the geometric series is a known convergent series, it has the property that given an $\epsilon > 0$, (fixed, but arbitrary), there exists an N such that when

$$R_s = |S - S_N| < \epsilon \text{ when } N < n.$$

Let ϵ be the maximum permissible error. Then the number of terms needed in the series portion of Eqn. 2.14 to guarantee that terminating the series will not produce an error greater than ϵ, may be calculated as follows:

$$r^n\left(\frac{r}{1-r}\right) \leq \epsilon$$

$$r^n \leq \epsilon\left(\frac{1-r}{r}\right)$$

$$n \ln r \leq \ln[\epsilon(1-r)] - \ln r,$$

and finally,

$$n \geq \frac{\ln[\epsilon(1-r)]}{\ln r} - 1 .$$

Thus, in the geometric series, any termination after the integral number of terms greater than the calculated N, will generate an error less than the maximum permissible error.

Since our remainder is less than the corresponding remainder in the geometric series after n terms, our error will be less than the error generated by terminating the geometric series after n terms.